Diameter Scaling of the Optical Band Gap in Individual CdSe Nanowires

Anton Myalitsin,[†] Christian Strelow,[†] Zhe Wang,[†] Zhen Li,[†,‡] Tobias Kipp,[*,†] and Alf Mews[†]

[†]Institute of Physical Chemistry, University of Hamburg, 20146 Hamburg, Germany and [‡]ARC Centre of Excellence for Functional Nanomaterials, Australian Institute for Bioengineering and Nanotechnology, University of Queensland, Australia

ABSTRACT The diameter dependence of the optical band gap of single CdSe nanowires (NWs) is investigated by a combination of atomic force microscopy, scanning fluorescence microscopy, and transmission electron microscopy. We find a good congruence of the experimental data to calculations within the effective mass approximation taking into account quantization, exciton Coulomb interaction, and dielectric mismatch. The experimental data are furthermore compared to different theoretical approaches. We discuss the influence of alternating wurtzite and zinc blende segments along the NWs on their optical properties.

KEYWORDS: nanowires · CdSe · fluorescence · optical band gap · effective mass approximation

Over the past decade the optical and electronic properties of semiconductor NWs have been intensively investigated. In contrast to zero dimensional quantum dots, extended one-dimensional NWs have an advantage for use in possible electronic devices, because they can be contacted by macroscopic electrodes.[1] Direct band gap materials are of particular interest, since their optical and electrical properties can be exploited at the same time. Several pioneering studies have demonstrated the use of NWs, for example, as gain media for lasers,[2] gas sensors,[3] photo sensitizers for solar cells,[4] field-effect transistors,[5] or as probes for biological tissues.[6] However, their diameter is typically far above the Bohr radius.

With the catalyst-based solution–liquid–solid synthesis, NWs with diameters below the exciton Bohr radius have been prepared in larger quantities.[7] Such NWs are of special interest for devices based on their optical properties since the band gap is dependent on the diameter, which is relatively easy to tailor.[8–11] In fact, measurements on ensembles of NWs revealed an increase of absorption and photoluminescence (PL) peak energies with decreasing diameter.[8,11,12]

Structural and optical measurements on single NWs are advantageous to unfold properties that remain hidden in averaging experiments on ensembles. Such measurements revealed many interesting features, yet, not all of them are fully understood. For example, CdSe nanowires prepared with wet-chemical methods show structural fluctuations[9] as well as fluorescence intensity fluctuations along individual nanowires.[13] Variations in crystal structure (segments of wurtzite and zinc blende, with different band gaps and offsets) are reported to lead to a formation of separated quantum mechanical systems, which in turn results in "hot spots" in the PL signal,[13–15] with a blinking behavior similar to QDs as charge carriers localize in different sections in a wire. On the other hand, CdSe NWs have also been reported to behave like single quantum mechanical systems.[16,17] The interpretation of fluorescence data is further complicated by photobrightening effects in the presence of organic ligands,[18] by agglomerates of colloidal nanoparticles,[19] and by variations in ligand coverage that may lead to spectral heterogeneity as well as different emission intensities along the wire.[20]

In this work, we present a direct correlation of the structural and optical properties of one and the same individual CdSe NWs. In particular we measured the fluorescence of individual NWs to determine their optical band gap and performed highly accurate structural measurement by atomic force microscopy (AFM) and transmission electron microscopy (TEM) of the same NWs. We found that AFM measurements alone are not sufficient to decide whether the investigated nanostructure is a single one. Also we found that AFM might lead to a systematic error in determining the wire diameter. From the correlation of TEM and fluorescence data we obtained a complete set of data of the diameter-dependent optical band gap which is compared to predictions of several theoretical models. In particular, within the effective mass approximation, we separately discuss the effects of quantization, excitonic Coulomb interaction, and a dielectric mismatch between NW and its surrounding. Overall we obtain

* Address correspondence to kipp@chemie.uni-hamburg.de.

Received for review June 15, 2011 and accepted August 22, 2011.

Published online August 22, 2011
10.1021/nn202199f

a good coincidence of the theory with the experimental data. However, we show that shortcomings of the model itself make it very difficult to accurately trace back bulk parameters like the fundamental band gap energy and effective masses from our experimental data. We further compare our data to results of other theoretical models of NWs given in literature but do not find a better congruence.

RESULTS AND DISCUSSION

We used a standard procedure to synthesize the CdSe NWs[21] (for details see Methods). The NWs exhibited a diameter distribution centered at 11 nm with a standard deviation of $\sigma \approx \pm 3$ nm. Therefore thinner wires had to be purposefully selected in the experiments, and the data presented below does not directly reflect the actual size distribution of the samples. Without further conditioning most NWs form bundles and nanofibers upon deposition. Several parameters were tested to separate the wires. In short, ultrasonication debundles the wires, but also reduces their average length, also the number of fragments (CdSe NWs with length $< 1\ \mu$m) increases. Centrifugation was used to purify the sample and remove CdSe nanocrystal admixtures which are also formed during the synthesis. However, thinner wires are also more difficult to precipitate, therefore wires with a larger diameter are enriched with each cleaning step. Details on the NW deposition on silicon nitride membranes employed in this study that exhibit minimized (but not completely suppressed) bundling are given in Methods section.

Figure 1 shows a compilation of a scanning PL image, an AFM image, as well as TEM images of one and the same NW structure. From the PL image one might conclude that the emission stems from a single NW that exhibits some position dependent inhomogeneities of the PL emission, including some hot spots of strong emission. However, the AFM image reveals that the investigated structure is not necessarily a single NW. In fact, it becomes clear that, at least in the lower left part of the image, several NWs can contribute to the PL emission. The TEM images allow for a much closer look on the investigated structure. Here, clarified by the three magnified images, it becomes obvious that even when PL and AFM images might suggest the investigation of a single NW, mostly two or three adjacent NWs are investigated. The comparison of the different microscopy images demonstrates one difficulty in the investigation of individual NWs. From PL images alone, it is not possible to decide whether the emission stems from a single NW. Even the spectrally dispersed PL emission does not prove the investigated structure to be a single wire. On the one hand, for example, two adjacent NWs of the same size reveal a similar spectrum as the individual NW, on the other hand, the spectrum of two adjacent NWs of different diameter is not necessarily just the superposition of the individual NW because of, for example, energy transfer between the NWs. AFM images allow for a more reliable verification whether single NWs are investigated. However, due to the limited lateral resolution the assignment is not unambiguous when the NWs adjoin laterally, like it is mostly the case in Figure 1. TEM images allow for an unambiguous correlation of the PL data to the nanostructure(s) under investigation. However, there are two major drawbacks. First, TEM investigations require special and easily damageable substrates for the NWs, like carbon-coated copper grids or silicon nitride membranes. Second, TEM investigations drastically alter the optical properties of NWs. In fact, after TEM imaging, the NWs do not emit any measurable PL light anymore. Thus, the structural analysis of NW structures by TEM can only have been done after a thorough investigation of their optical properties.

To investigate the PL emission of single NWs and correlate it to their structural properties we applied the following workflow. We estimated the quality of our sample by first characterizing the sample with AFM. Despite the above-mentioned drawbacks of AFM, large agglomerates of NWs can be excluded for a more detailed investigation, and regions of interest with presumably single NWs can be identified. Then, these regions were found again and investigated by scanning fluorescence microscopy. A comparison between AFM and confocal scans showed that presumably individual NWs have weak PL and can be easily overlooked. In several cases the PL is below our detection limit. Then, the PL light of presumably single NWs has been recorded with spatial and spectral resolution for a later in-depth analysis. At last, these NW structures have been investigated by TEM.

The comparison of all three different microscopy methods reveals the following general results. Scanning PL images revealed the strongest spatial PL intensity variations along the investigated nanostructure for bundled NWs, whereas individual NWs appeared spatially more homogeneous. Figure 2 correlates the height of NWs as determined by AFM with their diameter as determined by TEM. The red line is a linear fit of the data proving that AFM typically overestimates the radius by about 3 nm. This is because the AFM height depends on the interaction between the sample and the tip, and is therefore influenced by the surface and possible ligands still attached to the NWs.[22]

Figure 3 exemplarily shows three PL spectra. The blue curve has been obtained from the bundled NWs of Figure 1 at a position depicted in panel d where three wires with diameters of 11.1, 10.0, and 6.9 nm, respectively, contribute. Both other spectra, peaking at smaller and larger energies, respectively, are obtained from single NWs, as verified by their TEM images shown in the insets. Their diameters are 17.5 and

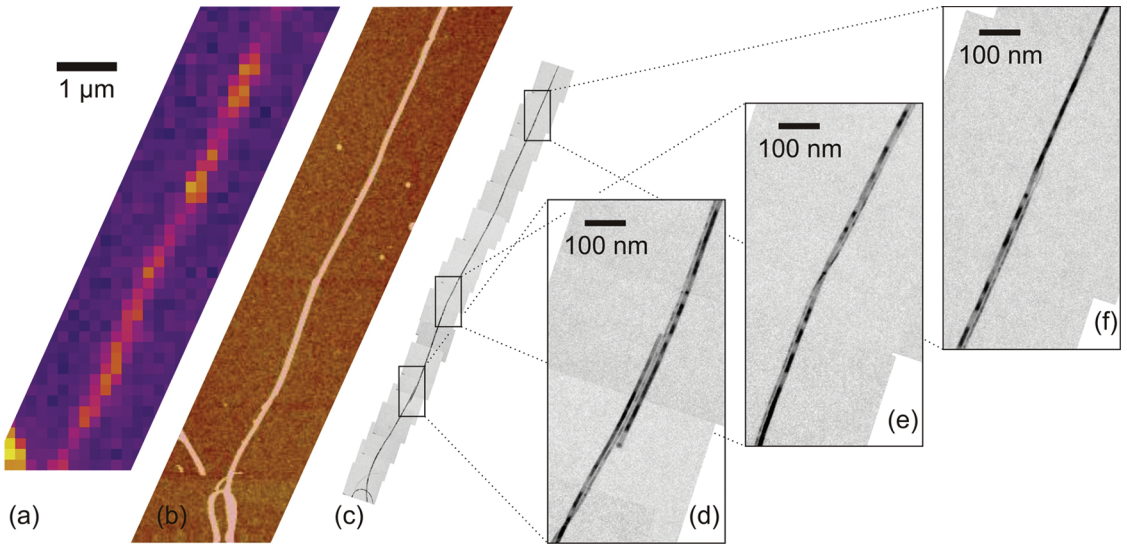

Figure 1. CdSe nanowires: (a) PL image from a confocal microscope, (b) AFM image of the same sample position, (c) stitched TEM images of the same sample position, (d−f) magnified areas marked in panel c. TEM images reveal that presumably single NWs, as judged from PL and AFM images are in fact bundles of NWs. Additionally, AFM overestimates the diameter of the NWs, for example, at the position of areas shown in panel d. AFM gives a height (thus diameter) of ∼14 nm, while the diameter determined from TEM for the three wires is 11.1, 10.0, and 6.9 nm.

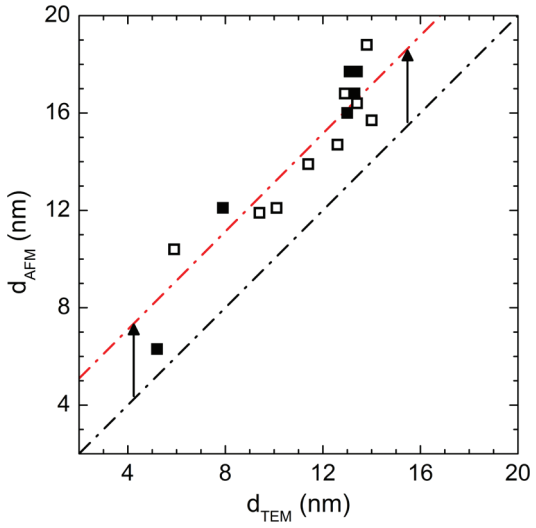

Figure 2. Comparison between diameters retrieved from AFM and TEM from the same individual nanowires. Solid squares are wires where luminescence was measured and which went into Figure 4a. The black dash-dotted line represents identical values. The red line is a linear fit of the experimental data. Compared to the black line it is essentially vertically shifted by 3 nm.

5.1 nm, respectively. Without the knowledge of the TEM images, the larger PL peak full width at half-maximum (fwhm) of the blue curve might already suggest bundled NWs, but its line shape does not allow to extract either the number of NWs or their respective maximum PL emission energy. All optical data used for our analysis below has been measured from individual NWs, as verified by TEM. The black and red spectra in Figure 3, together with their TEM images, represent the thickest and thinnest NW under investigation, respectively. The maximum PL emission energy strongly changes with the diameter of the NWs, as will be discussed in detail below. The typical PL fwhm is about 80−90 meV. The investigation of the temporal evolution of the PL light in consecutive time bins as small as 25 ms reveals intensity fluctuations of the order of 20% of the average intensity. These fluctuations may be attributed to a similar process as the well-known blinking of nanocrystals.[23] The rather large fwhm might originate from spectral shiftings in time, however, they have to occur on a time scale smaller than 200 ms, that is, the integration time of our spectrally resolved measurements. Furthermore, structural inhomogeneities of the NWs should contribute to a broadening. We estimated the diameter variations of the NWs by evaluating TEM images of several positions along each wire. We found typical standard deviations of ±0.3 nm for the whole range of different diameters. The effect of alternating crystal lattice modifications along the NWs will be addressed later.

The black circular data points in Figure 4a give the experimental results of the scaling of the optical band gap with the diameter of the NWs. Here, the maximum PL emission energy was determined by fitting the rather broad PL emission of a NW with a Gaussian. We estimate its error to be smaller than ±4 meV (see error bars). The optical band gap strongly increases with decreasing diameter.

We now want to compare the complete set of data of the diameter dependent optical band gap to predictions of different theoretical models. First, we intensively discuss to which extent the experimental data can be modeled within the effective-mass approximation that transfers fundamental properties of bulk to

the nanosized material and which is probably the most descriptive. The optical band gap can be regarded as composed of three different parts: (i) the diameter dependent quantization energy of electrons and holes due to the reduced size, (ii) the exciton Coulomb energy due to attraction between an electron and a hole as well as interaction between charges and image charges induced by a dielectric mismatch, and (iii) the fundamental bulk band gap energy independent of the diameter.

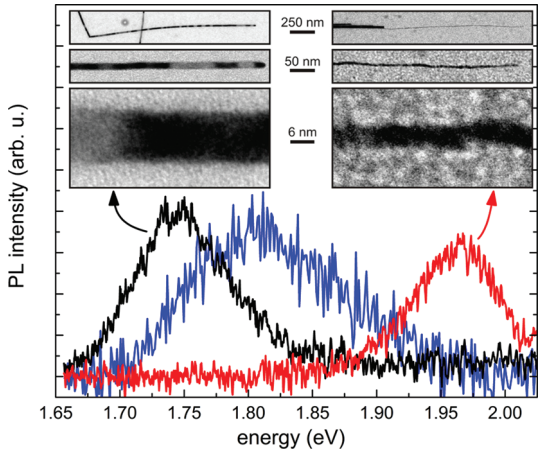

Figure 3. Blue curve: PL spectrum of three bundled NWs shown in Figure 1d with diameters of 11.1, 10.0, and 6.9 nm. Black and red curve: Single NW PL spectra of the thickest (black) and thinnest (red) NW under investigation. The insets show their TEM images of different magnifications. Here, differences in contrast may stem from changes in diffraction conditions, either by a rotation of a the stacking plane along the wire axis or by slightly shifting out of the beam focus. Another explanation may be charging of the sample.

The upper panel of Figure 4b depicts the diameter-dependent quantization energy E_{quant} for a cylindrical CdSe NW. The red curve represents the analytic solution of the Schrödinger equation for infinite barriers, $E_{quant} = (2\hbar^2\beta_0^2)/(\mu d^2)$, where d is the diameter, $\beta_0 = 2.4048$ is the first root of the Bessel function J_0, and μ is the reduced effective exciton mass $\mu = (m_e m_h)/(m_e + m_h)$. For the effective electron and hole masses we assumed bulk values $m_e = 0.12m_0$ and $m_h = 0.5m_0$ (*cf.* refs 24 and 25). The reality should be better described when finite barriers are assumed. We numerically solved the corresponding Schrödinger equation setting the barrier height to $U = 5$ eV,[26] assuming the above given effective masses, and applying Ben Daniel-Duke boundary conditions for the wave functions at the semiconductor/air interface.[27−29] The results of these calculation are given as the black curve in the upper panel of Figure 4b. E_{quant} strongly depends on the NW diameter, the different barrier heights most strongly alter E_{quant} for small diameters, and even for

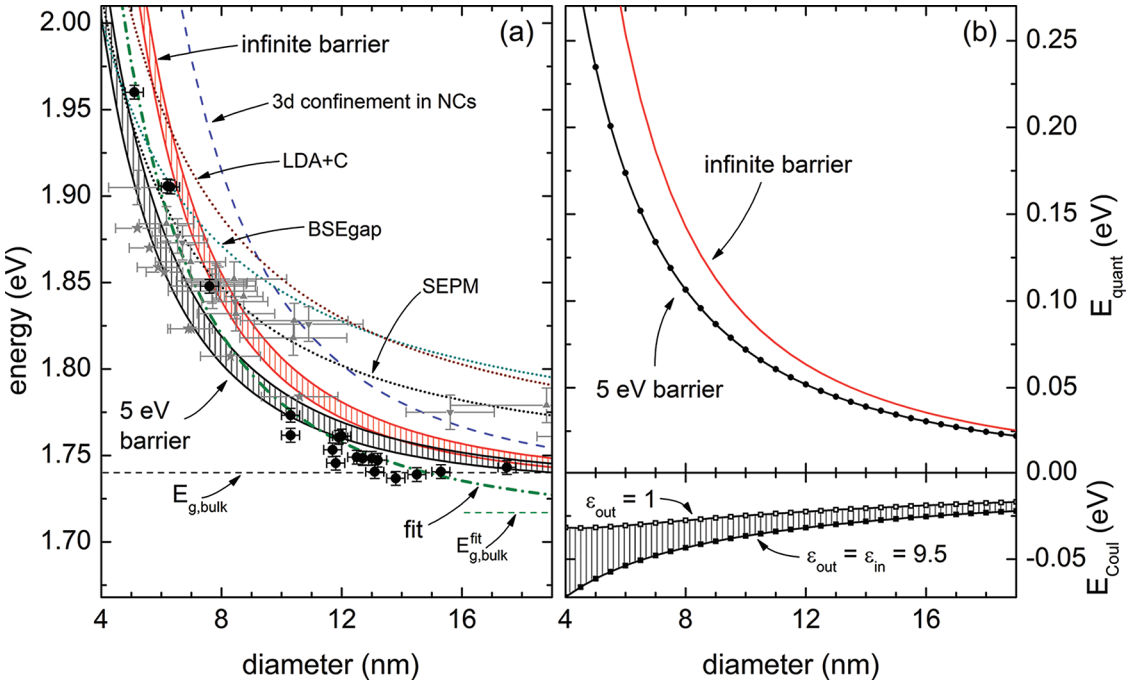

Figure 4. (a) Scaling of the optical band gap with the NW diameter. Black circular data points represent the experimental results. The lines represent model calculations. The red and black solid lines are results of the effective mass approximation (EMA), regarding the NW as a potential well with infinite (red) or finite (height ≈ 5 eV, black) barriers. The lower line of both groups is calculated assuming no dielectric mismatch (*i.e.*, $\varepsilon_{out} = \varepsilon_{in} = 9.5$) while for the upper curve $\varepsilon_{in} = 9.5$ and $\varepsilon_{out} = 1$ is assumed. These curves result from adding E_{quant}, E_{Coul}, and $E_{g,bulk}$. The green dash-dotted line represents results of the EMA obtained with fitted parameters (see text). For comparison, the blue dashed line shows the scaling of the optical band gap for spherical nanocrystals within the EMA. The dotted lines represent results of different theoretical models reported in literature (see text). Gray data points represent experimental results taken from ref 8 (absorption, triangles) and ref 11 (PL, stars). (b) EMA calculation of E_{quant} for infinite and finite potential barriers (upper panel) and E_{Coul} with and without dielectric mismatch.

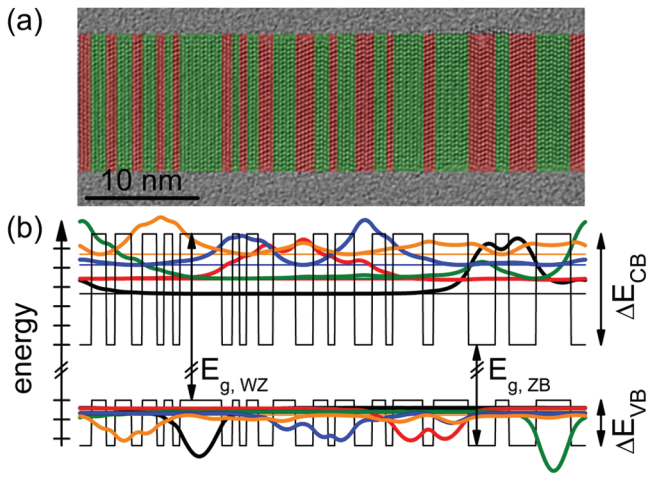

Figure 5. (a) Typical high-resultion TEM image of a NW revealing alternating crystal modifications. Wurtzite (zinc blende) segments are colored green (red). (b) Scheme of the corresponding type-II potential of conduction and valence band (black), calculated lowest electron and hole eigenenergies (colored horizontal lines), and, attached to the latter, the corresponding squared wave functions. For the calculation, ΔE_{CB} = 144 meV and ΔE_{VB} = 59 was assumed. The spacing of the energy tick marks is 25 meV.

diameters as large as 20 nm E_{quant} is not negligibly small.

The Coulomb energy of electrons and holes in a cylindrical NW without and with consideration of a mismatch of the dielectric permittivity inside and outside of the NWs has been investigated in depth by Slachmuylders and co-workers in refs 30 and 31. By adiabatically separating the lateral motion of the particles from the motion along the NW and assuming infinite barrier heights for the lateral potential, they were able to set up an one-dimensional Schrödinger equation for the relative exciton coordinate containing an effective exciton potential. This potential includes terms (i) for the direct Coulomb interaction between electron and hole, as well as (ii) for the self-energy contribution from the interaction between an induced image charge and the original charge, and (iii) for the induced contribution from the interaction between a charge in the NW and the induced image charge. They studied each term in dependence of the wire radius and dielectric mismatch and fitted the results to analytical expressions, thus yielding one analytical formula for the effective exciton potential. We used this formula to numerically solve the corresponding Schrödinger equation and find the Coulomb energy in order to model our NWs. Note that, for one-dimensional excitons in CdSe nanorods, analytical expressions for the effective potential as well as for the eigenenergies and wave functions have also been given in ref 32. Here, we again assumed the above given effective masses. Furthermore, we assumed a relative permittivity of ε_{in} = 9.5 inside the CdSe NW (*cf.* ref 33) and distinguish between two cases, in which we either assume no dielectric mismatch, that is, $\varepsilon_{out} = \varepsilon_{in}$, or we set the permittivity outside the NW to that of vacuum, that is, $\varepsilon_{out} = 1$. The results of both model calculations are shown in the lower panel of Figure 4b. It can be seen that the absolute value of the Coulomb energy is smaller than the quantization energy; however, its impact is not negligible. The reality should be better described when the dielectric mismatch is taken into account, even though, since the NWs are deposited on a substrate and are at least partially surrounded by ligand molecules, the effective relative permittivity differs from the vacuum value. The dielectric mismatch leads, on the one hand, to a strengthening of the exciton binding energy due to interaction with the induced image charges, on the other hand, the self-energy of the charges is increased. Overall, the absolute value of the Coulomb energy is reduced.[31,34]

For the fundamental bulk band gap energy of CdSe we tentatively assume $E_{g,bulk}$ = 1.74 eV (*cf.* refs 25 and 35). Adding now $E_{g,bulk}$, E_{Coul}, and E_{quant} for the different model calculations we obtain theoretical values for the optical band gap that can be compared to the experimental data. Results are shown as solid lines in Figure 4a. The red (black) lines correspond to the infinite (finite) barrier model. In both cases, the dielectric mismatch is taken into account only for the upper curve. It can be seen that principally the model calculations follow our experimental data; however, significant deviations are visible. These deviations can be explained with intrinsic shortcomings of the two-band effective mass approximation itself, in particular for nanometer-sized structures, as well as by the uncertainty of the bulk parameters assumed for the calculation. For the effective electron and hole masses that essentially go into the calculation of E_{quant} as well for the relative permittivity that goes into E_{Coul} and even for the fundamental band gap $E_{g,bulk}$ several different values are given in literature.[25,35] We try to fit our experimental data within the above given model assuming finite barrier heights for the calculation of

E_{quant} and strong dielectric mismatch ($\varepsilon_{out} = 1$) for the calculation of E_{Coul}. Starting with the parameters given above, we obtain a better congruence assuming by trend larger barrier heights, smaller effective masses and a smaller fundamental band gap. The dash-dotted curve in Figure 4(a) calculated for $m_e = 0.10m_0$, $U = 10$ eV and $E_{g,bulk}^{fit} = 1.717$ eV fits the experimental data quite well. We note that, since we have essentially four free fit parameters, the chosen set of parameters is not unique.

Typically, CdSe NWs grown by solution−liquid−solid method exhibit alternating lattice modifications, that is, wurtzite (WZ) and zinc blende (ZB), along their axes.[9,11] This is also the case for our NWs, as can be seen in the high-resolution TEM image in Figure 5a. Principally, these different phases complicate the above discussion of the optical band gap in NWs even more since they exhibit different band structures and, in particular, different electron affinities, ionization potentials, and fundamental band gaps.[13,14,36−38] Theoretical works reveal a smaller band gap of the ZB modification in the range of $\Delta E_g = 46−85$ meV, as well as conduction band (CB) and valence band (VB) offsets of $\Delta E_{CB} = 76−144$ meV and $\Delta E_{VB} = 30−59$ meV, respectively, leading to a staggered type-II potential along the NW with CB minima in the ZB segments and VB band maxima in the WZ segments.[36−38] Such a potential, corresponding to the TEM image, is sketched in Figure 5b.

We now want to discuss its implications on the optical properties of NWs. First of all, one might assume that the type-II potential along the wire leads to an effective confinement of charge carriers also along the NW. To enlighten this point we calculated the lowest electron and hole eigenenergies and corresponding wave functions for the sketched potential within the effective mass approximation by numerically solving the Schrödinger equation. We note that here we disregard Coulomb attraction between electrons and holes. For the model calculations we assumed the largest of above given theoretically predicted band offsets[38] of $\Delta E_{CB} = 144$ meV and $\Delta E_{VB} = 59$ meV since this should generate the strongest axial confinement. We chose periodic boundary conditions to account for the much larger length of the real NW compared to the TEM image detail. As a result, the horizontal lines in Figure 5b represent the five lowest electron and hole eigenenergies of the CB and VB potential, respectively. Attached to the eigenenergies also the corresponding squared wave functions are drawn. For the CB, the energy spacing between neighboring eigenstates is smaller than the thermal energy at room temperature ($kT \approx 25$ meV = spacing of energy tick marks) and the corresponding wave functions do considerably overlap. The same holds for the VB, where the wave functions are less expanded but the energy spacing is much smaller. Thus, our model calculations reveal that the different ZB and WZ segments are too short to effectively trap charge carriers, at least at room temperature. In this context, to clarify the point of an axial carrier confinement in more detail, we compare our experimental data with the theoretical optical band gap of spherical CdSe nanocrystals treated in the effective mass approximation including Coulomb attraction, $E = E_{g,bulk} + 2\hbar^2\pi^2/(\mu d^2) - 1.8e^2/(2\pi\varepsilon\varepsilon_0 d)$, as obtained by Brus[39] (dashed line in Figure 4a). The three-dimensional confinement in QDs reveals a much stronger energy increase with decreasing diameter than our NW data. This is a strong hint for a two-dimensional confinement in our NWs, thus a true quantum wire behavior, as has been extensively discussed in refs 8 ,40 and 41.

A second implication of the staggered type-II potential concerns the effective fundamental band gap of the NW. Depending on the band alignment of WZ and ZB segments and on their mean widths, it differs from the bulk band gap of the pure WZ or ZB phase. Assuming the above given band offsets, Figure 5b reveals that the effective band gap is smaller than the fundamental WZ band gap (up to 70 meV) but larger than the fundamental ZB band gap.

Closely related, a third implication of the type-II potential affects the PL emission line width. The modeled potential in Figure 5b has an overall length of about 45 nm, while the PL measurements probe the NW underneath the excitation laser spot of at least about 250 nm. On this rather large length scale, the statistical nature of the segment lengths should indeed lead to an inhomogeneous broadening of the PL emission line making the experimentally measured line widths reasonable (*cf.* Figure 3).

We now want to compare our experimental data with results from other theoretical approaches that model the electronic properties of semiconductor NWs, different from the above-discussed effective-mass approximation. Particularly, we compare our results with the theoretical results of three papers by (i) H. Yu *et al.*,[8] (ii) J. Li and L. W. Wang,[42] and (iii) J. G. Vilhena *et al.*[43] In the first paper the so-called plane-wave semiempirical pseudopotential method (SEPM) is exploited. The authors calculated the increase in the band gaps of CdSe quantum wires within the diameter range of $d = 1.39−13.25$ nm over the bulk value for CdSe assumed to be $E_{g,bulk} = 1.74$ eV. They empirically fitted their theoretical results and found an $E = E_{g,bulk} + 1.82\ \text{eV}/(d(\text{nm}))^{1.36}$ dependence for the band gap energy.[8] We included this result in Figure 4a as the dotted-line labeled SEPM. For large diameters it overestimates the experimental PL data; however, we note that no Coulomb interaction has been explicitly taken into account in the calculations. The increase of the energy with decreasing diameter is considerably smaller in the theory compared to our experimental results. In the second paper *ab initio* calculations have been performed using density functional theory under local

density approximation in which the bulk effective mass is corrected to fit with experimental values (LDA+C). This approach should yield good values for the diameter-dependent confinement energies, while the obtained absolute band gap energy should be corrected by a constant value to fit with the bulk band gap.[42] The authors calculated confinement energies and explicitly included electron−hole Coulomb interaction for diameters between 1.36 and 4.37 nm, empirically fitted their results, and found a $E = E_{g,bulk} + 1.95$ eV/(d(nm))$^{1.24}$ dependence. Assuming again $E_{g,bulk}$ = 1.74 eV, we included this result in Figure 4a as the dotted line labeled LDA+C even though, strictly speaking, these results have been obtained for a diameter range smaller than the one accessible in our experiment. The curve generally lies above our experimental data; however, its slope fits the experiments better than the SEPM results. The third paper reports on a first-principle approach beyond density functional theory. The authors used the so-called GW method for the band structure and the Bethe−Salpeter equation for optical absorption and interpolated their results for the optical band gaps by E = 1.74 eV + 1.05 eV/d(nm). We included this result in Figure 4a as the dotted line labeled BSEgap. It does not reproduce our experimental results better than the aforementioned models.

Finally, we want to compare our experimental data with existing experimental literature data, in particular that of W. E. Buhro and co-workers. The small gray triangles and stars in Figure 4a represent the band gap absorption data and PL data given in ref 8 and ref 11, respectively. These data sets have been obtained in ensemble measurements, their energy offset can be explained by a Stokes shift between absorption and emission. The comparison to our experimental data reveals no complete consistency. The diameter-dependent slope of our data points is larger than the reported ones. Reasons for this discrepancy, for example, different NW syntheses or investigation methods, cannot unambiguously be clarified by now. In this context we want to note that a possible Stokes shift in NWs is not considered in aforementioned theoretical models, particularly in the two-band effective mass approximation. Such a Stokes shift, however, if more or less constant for different diameters, does not carry too much weight compared to the uncertainty of the actual bulk band gap assumed for the NWs.

CONCLUSION

We correlate confocal fluorescence microscopy, AFM, and TEM measurements to investigate the optical band gap of *single* CdSe NWs. The correlation reveals that neither fluorescence microscopy alone nor its combination with AFM allows for an unambiguous identification of single NWs. After optical measurements, the evidence of single NWs can be provided by TEM measurements which also give accurate values of the diameter of the NWs. This is in contrast to AFM height measurements which overestimates the diameter typically by 3 nm. Measurements of the optical band gap of *single* NWs exhibiting different diameter are compared to different model calculations. We find a good congruence of the experimental data to calculations within the effective mass approximation taking into account quantization, exciton Coulomb interaction, and dielectric mismatch, as well as effects resulting from alternating wurtzite and zinc blende segments along the NW. However, deviations between experiment and calculations also demonstrate the shortcomings of the model itself. A comparison of the data to results of different theoretical approaches given in literature does not reveal any better congruence.

METHODS

The preparation of CdSe nanowires was based on the previous report.[21] In brief, a mixture of CdO, TOPO, and octanoic acid was dried and degassed under vacuum for 1 h at 100 °C. Then the vessel was filled with N_2 and the temperature was raised to 300 °C. When CdO was completely dissolved, the system was adjusted to 250 °C. Afterward a mixture of Bi nanoparticles and TOPSe was quickly injected into the vessel and the reaction was kept for 2 min before cooling down. Several milliliters of toluene were added to the solution to prevent the TOPO from solidifying. Then the nanowires were purified by using high-speed centrifugation (10000 rpm, 10 min).

Upon deposition NWs have a strong tendency to form bundles. Best results were achieved by the following method: 100 μL of a stock solution of CdSe nanowires was diluted with CH_2Cl_2 to 1 mL and centrifuged for 2 min at 18000 rpm. The overlaying solution was decanted and the process was repeated two more times. Afterward the suspension was treated with ultrasound for 5 min and 3−4 ultrasound pulses at 40 W. A 20 μL portion of the suspension was withdrawn and spin-coated at approximately 5000 rpm on a silicon nitride membrane (50 nm thickness). Prior to deposition a few drops of DI water and subsequent dichloromethane were spin-coated on the surface to remove potential remaining contaminants. Corners of the silicon nitride membrane were used to locate the same NWs in different setups (confocal, AFM, TEM).

AFM images were taken with a DI Nanoscope III and a JPK Nanowizard II. Transmission electron microscopy was performed with a JEOL JEM 1011 at an acceleration voltage of 100 kV on silicon nitride membranes. HRTEM images were taken on a JEOL JEM 2200 FS (UHR) with CESCOR and CETCOR corrector at an acceleration voltage of 200 kV on a copper grid with a carbon film.

All optical measurements were performed with a home-built confocal laser-scanning inverted microscope. For excitation an Ar-laser (514.5 nm, 2.41 eV) was focused with a high numerical aperture Zeiss Epiplan Apochromat objective (150×, NA = 0.95) to a diffraction-limited spot on the sample. The emitted PL light was collected by the same objective and detected either by an avalanche photodiode (PerkinElmer SPCM-AQR-W4) for PL imaging or by a back-illuminated EMCCD camera (Princeton Instruments, PhotonMax 1024) after being dispersed by a grating spectrometer for spectral analysis.

Acknowledgment. The authors thank A. Kornowski for high resolution TEM measurements.

REFERENCES AND NOTES

1. Yu, G.; Lieber, C. M. Assembly and Integration of Semiconductor Nanowires for Functional Nanosystems. *Pure Appl. Chem.* **2010**, *82*, 2295–2314.
2. Agarwal, R. Heterointerfaces in Semiconductor Nanowires. *Small* **2008**, *4*, 1872–1893.
3. Chiang, K. C.; Wu, W.-Y.; Ting, J.-M. Enhanced Lateral Growth of Zinc Oxide Nanowires on Sensor Chips. *J. Am. Ceram. Soc.* **2011**, *94*, 713–716.
4. Lee, J. C.; Lee, W.; Han, S. H.; Kim, T. G.; Sung, Y. M. Synthesis of Hybrid Solar Cells Using CdS Nanowire Array Grown on Conductive Glass Substrates. *Electrochem. Commun.* **2009**, *11*, 231–234.
5. Javey, A.; Nam; Friedman, R. S.; Yan, H.; Lieber, C. M. Layer-by-Layer Assembly of Nanowires for Three-Dimensional, Multifunctional Electronics. *Nano Lett.* **2007**, *7*, 773–777.
6. Timko, B.; Cohen-Karni, T.; Qing, Q.; Tian, B.; Lieber, C. Design and Implementation of Functional Nanoelectronic Interfaces with Biomolecules, Cells, and Tissue Using Nanowire Device Arrays. *IEEE Trans. Nanotechnol.* **2010**, *9*, 269–280.
7. Kuno, M. An Overview of Solution-Based Semiconductor Nanowires: Synthesis and Optical Studies. *Phys. Chem. Chem. Phys.* **2008**, *10*, 620–639.
8. Yu, H.; Li, J. B.; Loomis, R. A.; Gibbons, P. C.; Wang, L. W.; Buhro, W. E. Cadmium Selenide Quantum Wires and the Transition from 3D to 2D Confinement. *J. Am. Chem. Soc.* **2003**, *125*, 16168–16169.
9. Grebinski, J. W.; Hull, K. L.; Zhang, J.; Kosel, T. H.; Kuno, M. Solution-Based Straight and Branched CdSe Nanowires. *Chem. Mater.* **2004**, *16*, 5260–5272.
10. Li, Z.; Kornowski, A.; Myalitsin, A.; Mews, A. Formation and Function of Bismuth Nanocatalysts for the Solution–Liquid–Solid Synthesis of CdSe Nanowires. *Small* **2008**, *4*, 1698–1702.
11. Wang, F. D.; Buhro, W. E. An Easy Shortcut Synthesis of Size-Controlled Bismuth Nanoparticles and Their Use in the SLS Growth of High-Quality Colloidal Cadmium Selenide Quantum Wires. *Small* **2010**, *6*, 573–581.
12. Puthussery, J.; Kosel, T. H.; Kuno, M. Facile Synthesis and Size Control of II–VI Nanowires Using Bismuth Salts. *Small* **2009**, *5*, 1112–1116.
13. Protasenko, V. V.; Hull, K. L.; Kuno, M. Disorder-Induced Optical Heterogeneity in Single CdSe Nanowires. *Adv. Mater.* **2005**, *17*, 2942.
14. Robel, I.; Bunker, B. A.; Kamat, P. V.; Kuno, M. Exciton Recombination Dynamics in CdSe Nanowires: Bimolecular to Three-Carrier Auger Kinetics. *Nano Lett.* **2006**, *6*, 1344–1349.
15. Glennon, J. J.; Tang, R.; Buhro, W. E.; Loomis, R. A.; Bussian, D. A.; Htoon, H.; Klimov, V. I. Exciton Localization and Migration in Individual CdSe Quantum Wires at Low Temperatures. *Phys. Rev. B* **2009**, *80*, 081303.
16. Glennon, J. J.; Tang, R.; Buhro, W. E.; Loomis, R. A. Synchronous Photoluminescence Intermittency (Blinking) along Whole Semiconductor Quantum Wires. *Nano Lett.* **2007**, *7*, 3290–3295.
17. Glennon, J. J.; Buhro, W. E.; Loomis, R. A. Simple Surface-Trap-Filling Model for Photoluminescence Blinking Spanning Entire CdSe Quantum Wires. *J. Phys. Chem. C* **2008**, *112*, 4813–4817.
18. Biju, V.; Kanemoto, R.; Matsumoto, Y.; Ishii, S.; Nakanishi, S.; Itoh, T.; Baba, Y.; Ishikawa, M. Photoinduced Photoluminescence Variations of CdSe Quantum Dots in Polymer Solutions. *J. Phys. Chem. C* **2007**, *111*, 7924–7932.
19. Wang, S.; Querner, C.; Fischbein, M. D.; Willis, L.; Novikov, D. S.; Crouch, C. H.; Drndic, M. Blinking Statistics Correlated with Nanoparticle Number. *Nano Lett.* **2008**, *8*, 4020–4026.
20. Mintairov, A. M.; Herzog, J.; Kuno, M.; Merz, J. L. Near-Field Scanning Optical Microscopy of Colloidal CdSe Nanowires. *Phys. Status Solidi (b)* **2010**, *247*, 1416–1419.
21. Li, Z.; Kurtulus, O.; Fu, N.; Wang, Z.; Kornowski, A.; Pietsch, U.; Mews, A. Controlled Synthesis of CdSe Nanowires by Solution–Liquid–Solid Method. *Adv. Funct. Mater.* **2009**, *19*, 3650.
22. Ebenstein, Y.; Nahum, E.; Banin, U. Tapping Mode Atomic Force Microscopy for Nanoparticle Sizing: Tip-Sample Interaction Effects. *Nano Lett.* **2002**, *2*, 945–950.
23. Nirmal, M.; Dabbousi, B. O.; Bawendi, M. G.; Macklin, J. J.; Trautman, J. K.; Harris, T. D.; Brus, L. E. Fluorescence Intermittency in Single Cadmium Selenide Nanocrystals. *Nature* **1996**, *383*, 802.
24. Madelung, O., Rössler, U., Schulz, M., Eds. Cadmium Selenide (CdSe) Effective Masses, Fröhlich Coupling Constant, Hexagonal Modification; *Landolt-Börnstein—Group III Condensed Matter*; The Landolt-Börnstein Database Vol. 41B; SpringerMaterials.
25. Madelung, O., Rössler, U., Schulz, M., Eds. Cadmium Selenide (CdSe) Electronic Properties, Zincblende Modification; *Landolt-Börnstein—Group III Condensed Matter*; The Landolt-Börnstein Database Vol. 41B; Condensed Matter; SpringerMaterials.
26. Nethercot, A. H. Prediction of Fermi Energies and Photoelectric Thresholds Based on Electronegativity Concepts. *Phys. Rev. Lett.* **1974**, *33*, 1088–1091.
27. BenDaniel, D. J.; Duke, C. B. Space-Charge Effects on Electron Tunneling. *Phys. Rev.* **1966**, *152*, 683–692.
28. Brus, L. E. A Simple Model for the Ionization Potential, Electron Affinity, and Aqueous Redox Potentials of Small Semiconductor Crystallites. *J. Chem. Phys.* **1983**, *79*, 5566–5571.
29. Bastard, G. Wave Mechanics Applied to Semiconductor Heterostructures, Monographies de Physique; Wiley-Interscience: Paris, 1992.
30. Slachmuylders, A. F.; Partoens, B.; Magnus, W.; Peeters, F. M. Exciton States in Cylindrical Nanowires. *J. Phys.: Condens. Matter* **2006**, *18*, 3951.
31. Slachmuylders, A. F.; Partoens, B.; Magnus, W.; Peeters, F. M. Dielectric Mismatch Effect on the Exciton Sstates in Cylindrical Nanowires. *Phys. Rev. B* **2006**, *74*, 235321.
32. Shabaev, A.; Efros, A. L. 1D Exciton Spectroscopy of Semiconductor Nanorods. *Nano Lett.* **2004**, *4*, 1821–1825.
33. Madelung, O., Rössler, U., Schulz, M., Eds. Cadmium Selenide (CdSe) Dielectric Constants; *Landolt-Börnstein—Group III Condensed Matter*; The Landolt-Börnstein Database Vol. 41B; SpringerMaterials.
34. Bartnik, A. C.; Efros, A. L.; Koh, W.-K.; Murray, C. B.; Wise, F. W. Electronic States and Optical Properties of PbSe Nanorods and Nanowires. *Phys. Rev. B* **2010**, *82*, 195313.
35. Madelung, O., Rössler, U., Schulz, M., Eds. Cadmium Selenide (CdSe) Energy Gaps, Hexagonal Modification; *Landolt-Börnstein—Group III Condensed Matter*; The Landolt-Börnstein Database Vol. 41B; SpringerMaterials.
36. Murayama, M.; Nakayama, T. Chemical Trend of Band Offsets at Wurtzite/Zinc-Blende Heterocrystalline Semiconductor Interfaces. *Phys. Rev. B* **1994**, *49*, 4710–4724.
37. Wei, S.-H.; Zhang, S. B. Structure Stability and Carrier Localization in CdX (X = S, Se, Te) Semiconductors. *Phys. Rev. B* **2000**, *62*, 6944–6947.
38. Li, J. Wang, Shape Effects on Electronic States of Nanocrystals. *Nano Lett.* **2003**, *3*, 1357–1363.
39. Brus, L. Electron–Electron and Electron–Hole Interactions in Small Semionductor Crystallites: The Size Dependence of the Lowest Excited Electronic State. *J. Chem. Phys.* **1984**, *80*, 4403.
40. Yu, H.; Li, J.; Loomis, R. A.; Wang, L.-W.; Buhro, W. E. Two- *versus* Three-Dimensional Quantum Confinement in Indium Phosphide Wires and Dots. *Nat. Mater.* **2003**, *2*, 517–520.
41. Wang, F. D.; Yu, H.; Jeong, S. H.; Pietryga, J. M.; Hollingsworth, J. A.; Gibbons, P. C.; Buhro, W. E. The Scaling of the Effective Band Gaps in Indium–Arsenide Quantum Dots and Wires. *ACS Nano* **2008**, *2*, 1903–1913.
42. Li, J.; Wang, L.-W. Band-Structure-Corrected Local Density Approximation Study of Semiconductor Quantum Dots and Wires. *Phys. Rev. B* **2005**, *72*, 125325.
43. Vilhena, J. G.; Botti, S.; Marques, M. A. L. Excitonic Effects in the Optical Properties of CdSe Nanowires. *Appl. Phys. Lett.* **2010**, *96*, 123106.